Geochimica et Cosmochimica Acta 407 (2025) 253–264

Contents lists available at ScienceDirect

Geochimica et Cosmochimica Acta

journal homepage: www.elsevier.com/locate/gca

Understanding the relationship between foraminiferal Mg/Ca and clumped isotope thermometers

Marion Peral [a,b,*], Thibaut Caley [a], Bruno Malaizé [a], Thomas Extier [a], Linda Rossignol [a], Héloïse Barathieu [a], Émilie Dassié [a], Franck Bassinot [c], Dominique Blamart [c], Mathieu Daëron [c]

[a] Univ. Bordeaux, CNRS, Bordeaux INP, EPOC, UMR 5805, F-33600 Pessac, France
[b] Archaeology, Environmental changes & Geo-Chemistry (AMGC), Vrije Universiteit Brussel, Brussels, Belgium
[c] Laboratoire des Sciences du Climat et de l'Environnement, LSCE/IPSL, CEA-CNRS-UVSQ, Université Paris-Saclay, Orme des Merisiers, F-91191 Gif-sur-Yvette Cedex, France

ARTICLE INFO

Associate editor: Weifu Guo

Keywords:
Paleothermometry
Pleistocene
Foraminifera

ABSTRACT

Reconstructions of past sea surface temperatures (SSTs) are essential for understanding long-term climate variability, yet different proxy methods can yield divergent results. In this study, we compare Mg/Ca-derived SSTs from *Globigerinoides ruber* sensu stricto and *Trilobatus sacculifer* with clumped isotope (Δ_{47}) SSTs measured on *G. ruber* s.s. from the same core, MD96-2048 (Indian Ocean), covering the last 1.25 million years (Ma). Using the same species and samples allows minimizing ecological and environmental biases. We find that Δ_{47}-derived SSTs are systematically colder than Mg/Ca-SSTs prior to 0.4 Ma, while both proxies agree well after this point. This offset is not explained by diagenetic alteration (as assessed via SEM), nor by corrections for seawater salinity, pH, or Mg/Ca composition. The Mg/Ca-SSTs from *T. sacculifer* are more consistent with Δ_{47}-SSTs in the older interval, but do not fully resolve the discrepancy. We found that the apparent Δ_{47}-based cooling before 0.4 Ma is not supported by seawater $\delta^{18}O$ estimates or other climate indicators. Our results suggest that Δ_{47}-derived SSTs may be affected by an unknown bias in older intervals, although a combination of multiple factors explored in this study could also contribute to the observed offset.

1. Introduction

Accurate past sea-surface temperature (SST) reconstructions are a crucial requirement to understand the climate mechanisms and to test numerical climate models of past climates. Different methods exist to estimate past SST. Among them, two are based on the geochemical or isotopic composition of foraminiferal tests. Foraminifers are monocellular organisms with a widespread global distribution, whose calcium carbonate tests are preserved in sedimentary archives. At the first order, the magnesium to calcium ratio (Mg/Ca) of foraminiferal tests is sensitive to changes in seawater temperature. It is one of the most widely used method for estimating paleo-temperatures over the Quaternary and decipher climatic processes. The Mg/Ca to SST conversion preferably requires species-specific calibrations. However, this so-called Mg/Ca-thermometer is also affected by secondary parameters, reflecting biological and/or physico-chemical biases. The Mg/Ca-SST is influenced by pH and to a lesser degree salinity (Nürnberg et al., 1996; Lea et al., 1999; Rosenthal et al., 1997, 2006; Lear et al., 2002; Anand et al., 2003; Elderfield et al., 2006; Marchitto et al., 2007; Kısakürek et al., 2008, Mathien-Blard and Bassinot, 2009; Gray et al., 2018; Gray and Evans, 2019). Moreover, since the temperature dependence relies partitioning of Ca and Mg between seawater and the calcitic shell, applying this method to periods older than ~1 million years (Ma) requires prior knowledge of past seawater Mg/Ca variations over time (e.g., Gothmann et al., 2015).

Over the past decade, applying clumped-isotope thermometry to foraminiferal shells has been used increasingly to reconstruct seawater temperatures. The carbonate clumped-isotope method (Δ_{47} hereafter) is based on the quantification of subtle statistical anomalies in the abundance of doubly substituted carbonate isotopologues ($^{13}C^{18}O^{16}O^{16}O^{2-}$). When relative isotopologue abundances are governed by thermodynamic equilibrium relationship, ^{13}C-^{18}O bonds are slightly more

* Corresponding author at: Univ. Bordeaux, CNRS, Bordeaux INP, EPOC, UMR 5805, F-33600 Pessac, France.
E-mail address: marion.peral@u-bordeaux.fr (M. Peral).

https://doi.org/10.1016/j.gca.2025.08.011
Received 15 February 2024; Accepted 9 August 2025
Available online 20 August 2025

abundant than for a purely random distribution of isotopes, and this effect increases as equilibration temperature decreases (Schauble et al., 2006; Ghosh et al., 2007). This relationship is independent of the $\delta^{18}O$ of water in which the calcification occurs. Methodological studies on clumped isotopes have found no evidence of vital effects (Tripati et al., 2010; Grauel et al., 2013; Peral et al., 2018; Piasecki et al., 2019; Meinicke et al., 2020), salinity effects (Grauel et al., 2013; Peral et al., 2018) nor pH effects (Peral et al., 2020) on foraminiferal Δ_{47}, making it a promising paleo-thermometer. However, main limitations lie in the time-consuming nature of clumped-isotope analyses, which require large quantities of carbonate material (i.e. least several mg) to reduce the uncertainties in the reconstructed temperatures to a meaningful level, generally resulting in a strict trade-off between precision and temporal resolution.

Both Mg/Ca and Δ_{47} thermometers are based on the same material (foraminiferal shells). They may therefore be biased equivalently by classical limitations of foraminifera-based tracers, such as sensitivity to lateral advection, seasonality, or living depths (especially if living depth may have changed over time; De Vleeschouwer et al., 2022). By comparing Mg/Ca and clumped isotope measured from the same samples and from the same species, we avoid such ecological and sedimentary effects. However, differences in the comparison between the two thermometers on modern foraminifera (core-tops) are observed and were explained by processes such as dissolution, metal oxide coatings or contamination, diagenesis and species vital effects that influence Mg/Ca-temperature calibrations (Breitenbach et al., 2018) and correction for salinity and pH biases in Mg/Ca (Peral et al., 2020). On deep time, only a few records comparing the two thermometers have been published (Leutert et al., 2020 on mid Miocene; Meinicke et al., 2021 over the last 5 Ma at low resolution, Van der Ploeg et al., 2023 on mid Eocene). Leutert et al. (2020) have interpreted the discrepancies between the two thermometers, with colder Δ_{47}-SST than Mg/Ca-SST, as resulting from changes in surface ocean pH, affecting Mg/Ca-SST estimations. Meinicke et al. (2021) found a good agreement between Δ_{47}- and Mg/Ca-SST only after applying a dissolution correction on Δ_{47} values. Van der Ploeg et al. (2023) observed slightly warmer Δ_{47}-SST than Mg/Ca-SST, and interpreted this discrepancy as resulting from dissolution, salinity, and pH effects on Mg/Ca. As can be seen from these works, the difference between the two thermometers varies from one study to another, making it difficult to conclude about the biases at play. Additional datasets from more recent time periods, with better constraints on seawater conditions, are needed to gain a clearer understanding of these discrepancies.

Here, we compare the two methods over the past 1.25 Ma based on measurements performed within the same samples and on the same planktonic species (*Globigerinoides ruber* sensu stricto), from core MD96-2048 retrieved in the Indian Ocean (660 m of water depth; near Delagoa Bight; 26°10′482″S, 34°01′148″E; Fig. 1). Our objectives are to assess whether there is a discrepancy between the Mg/Ca and the Δ_{47}-thermometers, and to determine whether our data are better suited to clearly identify the potential biases affecting one or both of these methods. We also compare our Mg/Ca data with those from the foraminifer species *Trilobatus sacculifer (T. sacculifer)*, a shallow-dweling species like *G. ruber* (Schiebel and Hemleben, 2017), but whose Mg/Ca ratios are known to be less affected by secondary effects.

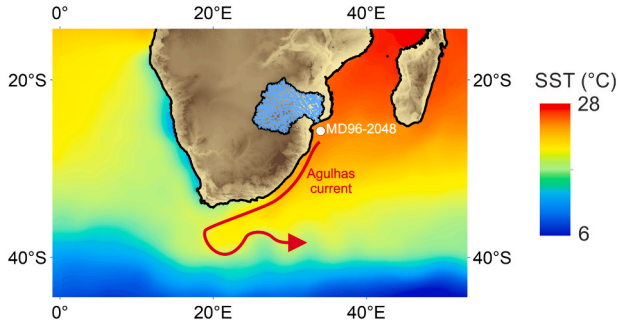

Fig. 1. Map of southwest Indian and Atlantic Oceans with location of the studied core. The map also includes the indication of the modern sea surface temperature distribution patterns in the Agulhas system, the location of Limpopo catchment (blue), the studied core (MD96-2048 – white dot) and a schematic views of the Agulhas current system (red).

2. Material and methods

2.1. Material

The studied area is today under the frequent influence of the Delagoa Bight lee eddy (Quartly and Srokosz, 2004; Lutjeharms, 2006; Lamont et al., 2010). It is also located beneath the present "precursor" (upstream) region of the Agulhas current and off the mouth of the Limpopo River (Fig. 1). The study was conducted on the top 23 m of the core MD96-2048. The chronology of this core has been published in Caley et al. (2018) by tuning the $\delta^{18}O$ benthic foraminifera record to the reference LR04 stack. One centimeter half round of the core was sampled and sieved for the foraminiferal based methods. The species *Globigerinoides ruber* sensu stricto (noted *G. ruber* s.s.), *Trilobatus trilobus* (*T. trilobus*) and *Trilobatus sacculifer* (*T. sacculifer*) were picked out for the analytical measurements. These species are shallow-dwelling species found in the upper 50 m of the ocean (Schiebel and Hemleben, 2017).

2.2. Clumped isotope method

The foraminifera were taken from the >150 um fraction of dry residue. The samples were selected based on the maximum $\delta^{18}O$ values of glacial-interglacial periods, associated to maximum and minimum changes of temperatures from previous Mg/Ca records (Caley et al., 2011,2018). Two surface-dwelling species of planktonic foraminifera have been taken for clumped isotope measurements. *G. ruber* s.s. has been studied for the full core and *T. trilobus* on the Holocene and Last Glacial maximum (LGM) to ensure good agreement between these surface-dwelling species over a glacial-interglacial cycle and to obtain reliable Δ_{47}-SST estimates for older glacial-interglacial cycles. The foraminifera were cleaned after crushing with water and methanol, as described in Peral et al. (2018).

A total of 23 clumped-isotope analyses were performed at the Laboratoire des Sciences du Climat et de l'Environnement (LSCE) using the same equipment and procedures as those described by Daëron et al. (2016). A total of 434 analyses has been performed, including 209 standards and 225 samples measurements, within 6 sessions of measurements (November 2017, February 2018, May 2018, October 2020 with 3 sessions). The external reproducibility of the Δ_{47} is 14.6 ppm. The samples were measured in random order and were replicated between 3 and 20 times. The replicates of the same sample were measured in different sessions to avoid a potential climatic effect in the measurements. Potential contaminations are tracking by monitoring mass 48 and mass 49.

In 2017 and 2018 sessions, all background measurements from a given analysis were used to determine a mass-specific relationship linking background intensity (Z_m) and total $m/z = 44$ intensity (I_{44}): $Z_m = a + bI_{44}$. In 2020, all background measurements from a given session were then used to determine a mass-specific relationship linking background intensity (Z_m), total $m/z = 44$ intensity (I_{44}), and time (t): $Z_m = a + bI_{44} + ct + dt^2$. Background-corrected ion current ratios (δ_{45} to δ_{49}) were converted to $\delta^{13}C$, $\delta^{18}O$, and "raw" Δ_{47} values using the IUPAC oxygen-17 correction parameters (Brand et al., 2010; Daëron et al., 2016; Schauble et al., 2006). The isotopic composition ($\delta^{13}C$, $\delta^{18}O$) of our working reference gas was computed based on the nominal isotopic composition of carbonate standard ETH-3 (Bernasconi et al., 2018) and an oxygen-18 acid fractionation factor of 1.00813 (Kim et al., 2007). Raw Δ_{47} values were then converted to the "absolute" Δ_{47} reference

frame defined by the "ETH" carbonate standards (Bernasconi et al., 2021) using the pooled regression approach (Daëron, 2021) as implemented by the D47crunch Python library. Full analytical errors are derived from the external reproducibility of unknowns and standards and conservatively account for the uncertainties in raw Δ_{47} measurements as well as those associated with the conversion to the "absolute" Δ_{47} reference frame.

Recently, Fiebig et al. (2024) reported potential contamination in the ETH-3 standard. To test this, we measured leftover ETH-3 powder from various periods spanning from 2017 to the present and compared the results to a bleached ETH-3 sample used as a contamination-free reference. No significant differences were observed between the recent and older ETH-3 powders and the bleached reference, indicating that this contamination effect is absent from our dataset (Fig. 2).

The average Δ_{47} values for each sample are converted into temperatures using the updated calibration of Daëron and Gray (2023, eq. 5), combining Peral et al. (2018) and Meinicke et al. (2020) planktic calibration data. Both analytical and calibration uncertainties are propagated to calculate the final uncertainties on the temperatures derived.

To reconstruct the $\delta^{18}O$ of the seawater ($\delta^{18}Osw$), we combined the clumped isotope-temperatures with the $\delta^{18}O$ data, both obtained simultaneously, using Daëron and Gray (2023) equation based on Mulitza et al. (2003) data on *G. ruber*. The final uncertainties are calculated by propagating the analytical uncertainties of both Δ_{47}-derived temperatures and $\delta^{18}O$ values, as well as the equations uncertainties.

2.3. Mg/Ca measurements

The Mg/Ca measurements are presented in Caley et al. (2011,2018). A total of 25 specimens of *G. ruber* s. s. were picked within the 250–315 um size fraction, every 2–5 cm for trace element analyses. The shells were cleaned following the procedure of Barker et al. (2003). Briefly, after crushing, shells were cleaned to eliminate contamination from clays and organic matter and we applied a single leach procedure with weak acid before dissolving and analyzing the samples.

Here, we estimated the final temperatures using 4 different methods:

- ***Method 1:*** We used the mono-species equation of Anand et al. (2003) (equation for *G. ruber*, in Anand et al., 2003; with the parameter A in the calibration not assumed). Both analytical and calibration uncertainties (on constant A and B) were propagated to calculate the final errors on temperature.

$$Mg/Ca = 0.34\ (\pm 0.08)\ x\ \exp(0.102\ (\pm 0.01)\ x\ T)$$

With T for temperature in degrees Celsius.

- ***Method 2:*** We calculated the Mg/Ca-derived temperatures corrected for salinity and pH with the generic *G. ruber* equation defined by Gray and Evans (2019). However, this corrected Mg/Ca curve is available only for the last 0.8 Ma, due to CO_2 reconstruction not available after 0.8 Ma, as the pH is estimated from ice core CO_2 measurements (deepest age reached by Antarctic ice-cores; Lüthi et al., 2008) over the last 0.8 Ma. Uncertainties were estimated following Gray and Evans (2019).

$$T = \frac{1}{0.061\ (\pm\ 0.05)}\ x\ \left[\ln(Mg/Ca_{foram}) - 0.036\ (\pm 0.006)\ x\ (S - 35) + 0.87\ (\pm\ 0.1)\ x\ (pH - 8) - 0.03\ (\pm 0.03)\right]$$

With T for temperature in degrees Celsius and S for salinity.

- ***Method 3:*** In order to apply Gray and Evans (2019) correction procedure before 0.8 Ma, we have estimated the pH and the local salinity, using the equation of Gray and Evans (2019). For the pH reconstructions, because no local pH reconstructions are available, we used the pH extracted from the boron isotope measurements from 0.8 Ma to 1.25 Ma (Chalk et al., 2017). For the salinity reconstruction, we used the present-day regional relationship between salinity and seawater composition in oxygen-18 ($\delta^{18}O_{sw}$) (Garcia et al., 2019; Zweng et al., 2019). This $\delta^{18}O_{sw}$ is obtained by combining the Δ_{47} and the $\delta^{18}O$ (see methodology in clumped isotope). The global contribution of ice-sheet changes over time on the $\delta^{18}O_{sw}$ reconstructions is corrected using the estimated contribution from Bintanja and Van de Wal (2008) to obtain a local $\delta^{18}O_{sw}$ signal. We calculated the final errors by propagating the analytical uncertainties on Mg/Ca and $\delta^{18}O$, uncertainties on the calibrations (Gray and Evans, 2019; and the relation between $\delta^{18}O$ and salinity) and on the pH reconstructions. The equation is the same than Method 2, but the salinity and the pH are estimated differently.
- ***Method 4:*** We added a correction for Mg/Ca_{sw} by modifying the equation of Gray and Evans (2019), as in Leutert et al. (2020), with local salinity, global pH and differences in the Mg/Ca_{sw} between past and present-day conditions as expressed by Evans and Müller (2012). We used a present-day value of 5.2 mmol/mol (Horita et al., 2002) and values from Gothmann et al. (2015) over the last 1.39 Ma, measured on corals.

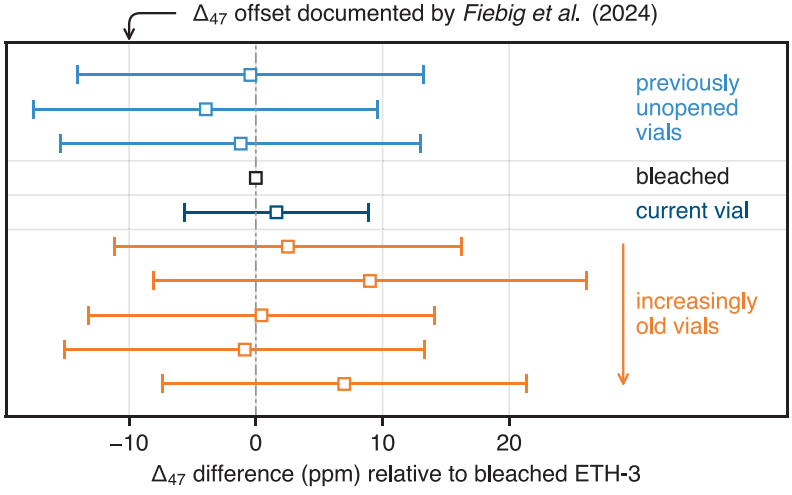

Fig. 2. Differences in ETH-3 Δ_{47} relative to bleached ETH-3 Δ_{47}, to test potential contamination in the ETH-3 standard, as reported in Fiebig et al. (2024). Bleached ETH-3 sample is used as a contamination-free reference, and compared to leftover ETH-3 powder from various periods spanning from 2017 to the present.

The corresponding expression for *G. ruber* is the following:

$$T = \frac{1}{0.061} \times \left[\ln\left(Mg/Ca_{foram} \times \frac{Mg/Ca_{sw,\ t0}^{H}}{Mg/Ca_{sw,t}^{H}}\right)\right] - 0.036 \times (S - 35) + 0.87 \times (pH - 8) - 0.03$$

with T for temperature in degrees Celsius. $Mg/Ca_{sw,t0}$ and $Mg/Ca_{sw,t}$ represent the Mg/Ca_{sw} at the present-day and in the past, respectively. H is the power component of Mg/Ca_{foram} and Mg/Ca_{sw} relationship as defined by Evans and Müller (2012). A H value of 0.79 is used based on calibration on *G. ruber* from Evans et al. (2016). In addition to the propagating uncertainties used in Method 3, we added the error on the Mg/Ca_{sw} and H estimations.

We also measured Mg/Ca on *T. sacculifer*, ranging between 250 and 315 μm size fraction. A total of 20–25 specimens were picked from 10 samples ranging between 0 and 1.2 Ma, to be analyzed with the ICP-OES at EPOC laboratory, University of Bordeaux. We followed the same cleaning protocol as for *G. ruber* based on Barker et al. (2003). The Mg/Ca values are converted into temperature using the equation of Gray and Evans (2019) for *T. sacculifer* (generic) and using local salinity reconstruction (see Section 2.2). We also derived the SST using the modified equation to include seawater Mg/Ca correction using H values from Evans et al. (2016) for *T. sacculifer*. No significant differences are noted between the two methods of SST estimate (<1 °C). We use the classic method from Gray and Evans (2019) for the manuscript.

3. Results

Overall, the Mg/Ca-SST values for *G. ruber* s.s. range from 26.4 to 22.3 °C (±2.8 °C 1SE) using Anand et al. (2003) calibration (Method 1) and 27.9 to 21.7 °C (±0.7 °C 1SE) using Gray and Evans (2019) equation (Method 2; Fig. 3). The Mg/Ca-SST values of *T. sacculifer* range from 24.5 to 21.5 °C (± 1.5 °C, 1SE; Fig. 3). The Δ_{47}-SST values range from 26.8 to 16.7 °C (±1.1 °C 1SE; Fig. 3). The MIS 6 is marked by very cold Δ_{47}-SST. The Grubbs test (Grubbs, 1969) does not consider this value to be an outlier ($p = 0.4389$). However, additional measurements would be necessary on adjacent samples to verify this cold temperature value.

The comparison between Mg/Ca-SST (*G. ruber* s. s.) and Δ_{47}-SST along the 1.25–0.4 Ma time interval shows a difference between the two thermometers, with colder Δ_{47}-SST than Mg/Ca-SST (Figs. 3 and 4). From 0.4 Ma to the Holocene, a good agreement is observed between the two thermometers, within the uncertainties (Fig. 4). Indeed, the violin plots show the distribution of the two methods that differs after 400 ka (Fig. 4.a). To evaluate the difference between the two distributions, the Wilcoxon signed rank test (Fig. 4.b) is used on different periods: 0–400 ka (Method 2 for Mg/Ca), 400–800 ka (Method 2 for Mg/Ca) and 400–1250 ka (Method 1 for Mg/Ca). This test evaluates the distribution of two matched samples and takes into account the error on the data by repeating 10,000 times the test for each period (each time adding random gaussian noise for each observation). 62.01 % of the tests for the periods 400–800 ka and 98.41 % for 400–1250 ka have a p-value inferior to 0.1, indicating that the null hypothesis is rejected and the distributions of Mg/Ca and Δ_{47} differ. At the opposite, for the 0–400 ka period, only 17.46 % of the tests (0.63 % without the MIS 6 samples) reject the null hypothesis. The results of the tests indicate that the two proxies follow the same distribution for the last 400 ka, but then differ of ~3.9 °C.

Over the Last Glacial Maximum (LGM), the Mg/Ca-SST (*G. ruber* s. s.; 22.5 ± 2.4 °C, 1SE) are similar, within the uncertainties, to the measured Δ_{47}-SST, independently of the selected foraminifera species (*G. ruber* s. s. (21.0 ± 1.2 °C) and *T. trilobus* (19.3 ± 1.4 °C)). The indistinguishable Δ_{47}-SST measured on both species, over a glacial-interglacial (G-IG) cycle suggests no change in living depth of these two surface-dwelling species at this time scale. At the core top level, both Mg/Ca-SST (24.1 ± 2.8 °C) and Δ_{47}-SST (on *G. ruber* s. s. (24.3 ± 1.2 °C) and *T. trilobus* (26.8 ± 1.3 °C)) are indistinguishable within the uncertainties (Fig. 3). They are also similar, within the uncertainties, to modern mean surface temperature found in the modern WOA-SST (24.9 °C ± 2.2 °C; World Ocean Atlas, WOA; Locarnini et al., 2018; Fig. 3).

The comparison between the Mg/Ca-SST of *T. sacculifer* and *G. ruber* shows good agreement overall, although some samples exhibit warmer Mg/Ca-SST values for *G. ruber* (Figs. 3 and 5.a). This discrepancy is unlikely to be linked to specific time periods, as deviations from the 1:1 line are observed in samples from both the 0–400 ka and 400–1200 ka intervals (Fig. 5.a).

In contrast, the comparison between Mg/Ca-SST from *T. sacculifer* and Δ_{47}-SST from *G. ruber* reveals a good agreement during the more recent 0–400 ka interval but indicates colder Δ_{47}-SST values over the 400–1200 ka interval (Fig. 5.b).

Comparisons between (a) Mg/Ca-SST on *T. sacculifer and* Mg/Ca on *G. ruber* s.s., and (b) Mg/Ca-SST on *T. sacculifer* and Δ_{47} on *G. ruber* s.s. Fewer data are available for comparison (a), as it relies on G. ruber Mg/Ca values corrected using pH estimates after 0.8 Ma, and these data are sporadically missing beyond that time (Method 4). Light blue corresponds to the recent interval until 400 ka, and dark blue to the older interval from 400 to 1200 ka. Uncertainties are plotted at 2 sigma.

4. Discussion

The first parts of the discussion focus exclusively on the comparison of thermometers within the same species to minimize potential biases related to seasonality, living depth, and other ecological factors. These

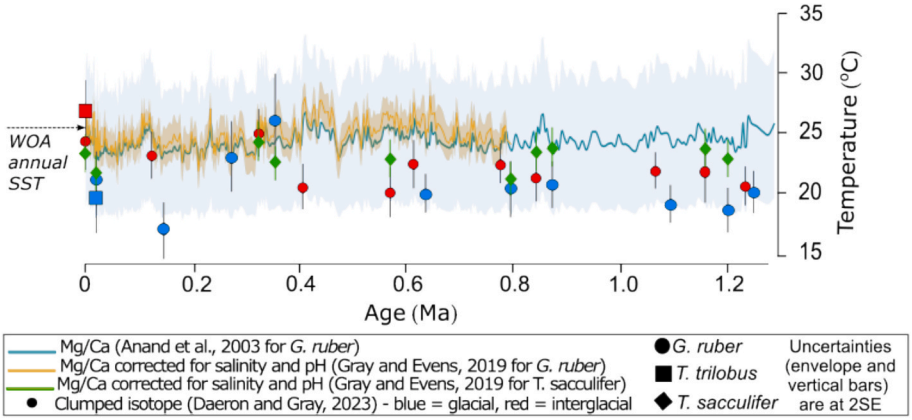

Fig. 3. Last 1.25 Ma of foraminiferal-based SST reconstructions record. Comparison between Mg/Ca-SST on *G. ruber* s. s. (in blue for Anand et al. (2003) calibration and orange for Gray and Evans (2019) calibration), Δ_{47}-SST performed on *G. ruber* s. s. (circle dot) and *T. trilobus* (square) and Mg/Ca-SST on *T. sacculifer* (green diamond). WOA = World Ocean Atlas. Uncertainties are at 2 sigma.

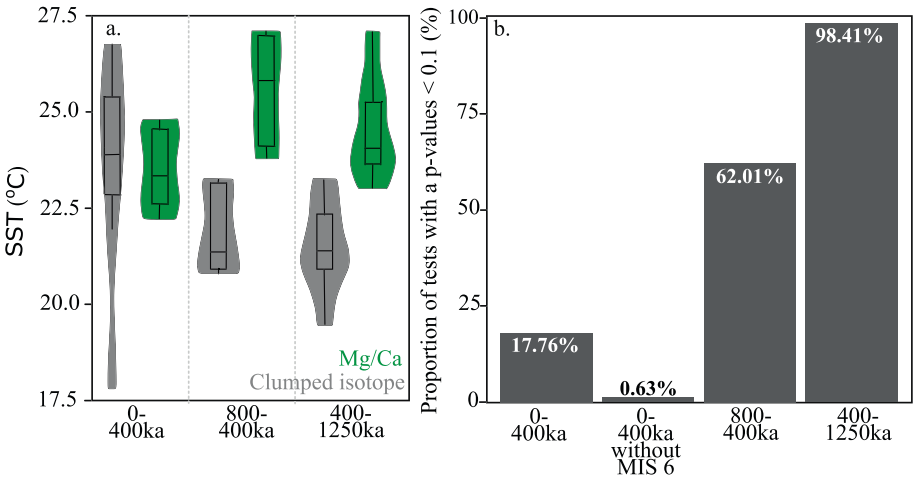

Fig. 4. Statistical test to evaluates the distribution of the two (Mg/Ca and Δ_{47} SST both on *G. ruber s. s.*) matched samples at different periods. Comparison between Mg/Ca-SST on *G. ruber* s. s. using (a) violin plot and (b) Wilcoxon signed rank test over the last 400 ka, from 400 to 800 ka and from 800 to 1250 ka. A distinction is made between these two last periods, because the uncertainties on Mg/Ca are larger in the oldest period (Method 1) than in the 400–800 ka period (Method 2).

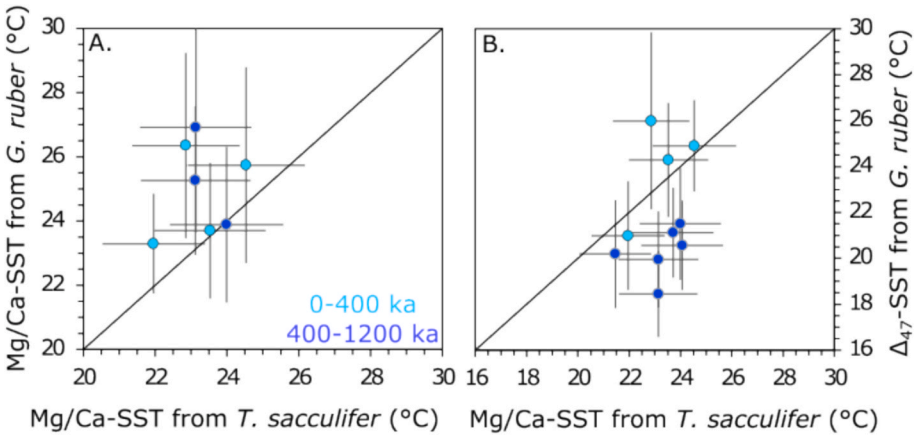

Fig. 5. Comparison between Mg/Ca and Δ_{47} SST for different species and at different periods.

parts explored well-known potential biases affecting the different proxies. The latter part shifts to comparisons with *T. sacculifer* to explore alternative hypotheses.

4.1. Foraminiferal size effect

We focus here on surface-dwelling species, but some species may live deeper in the water column during their lifetime. Depending on the size/life stage of the specimens, different temperatures may be recorded by the shells, corresponding to different water depths. The choice of foraminiferal size fraction is therefore crucial for geochemical proxies. It is important to study adult specimens that live primarily at the ocean surface rather than juveniles that may live in deeper layers. Also, small specimens of foraminifera can bias Mg/Ca results, and the ontogenetic influence on test size has been extensively studied for this proxy (e.g., Elderfield et al., 2002; Friedrich et al., 2012). Therefore, it is recommended to use foraminifers picked from a narrow size range for measurements. In contrast, Δ_{47} study on foraminifera showed no significant size effect in foraminifera (Peral et al., 2018), likely due to analytical uncertainties. In other words, while the effect may exist, it is too small to be detected within the uncertainties of Δ_{47}. Although such a potential size effect is hardly detectable, one cannot rule out completely the possibility that it can, to a certain extent, contribute to the differences observed between the two SST proxies. This effect could also be reflected in the $\delta^{18}O$ values, as different size fractions can reflect differences in living depths, seasons, or ontogenetic stages, leading to variations in $\delta^{18}O$.

To assess this, we compared the $\delta^{18}O$ values from the 250–315 μm size fraction measured by Caley et al. (2011) with those measured alongside Δ_{47} in the >150 μm fraction on the same species (*G. ruber* s.s) and same samples when data are available (Fig. 6). The results show a strong correlation ($R^2 = 0.92$) between the two $\delta^{18}O$ datasets, and follow well the line 1:1 (Fig. 6). This shows that, with respect to the oxygen isotope ratio, the size of the foraminifera is not an issue for our study.

4.2. Diagenetic/dissolution effects

Both Mg/Ca and Δ_{47} thermometers can be affected by diagenesis/dissolution of the foraminifera (Sexton et al., 2006; Meinicke et al., 2021; Leutert et al., 2019), which may lead to differences between the two thermometers, particularly over long-lasting records. In addition, Breitenbach et al. (2018) has shown on core tops samples that the differences between the two thermometers can be due to preservation (dissolution and diagenesis) and contaminations (metal coating/filling) issues that can affect both methods. However, it is important to note that isotopic methods can be more sensitive to micro-recrystallization than the Mg/Ca method (Staudigel et al., 2022). Here, the study site is shallow (660 m depth), limiting the likelihood of dissolution effects.

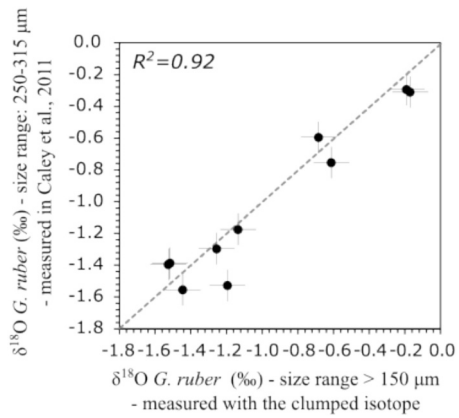

Fig. 6. Comparison of oxygen isotope data obtained for two different size ranges of *G. ruber*. The $\delta^{18}O$ measured with the clumped isotope on the fraction >150 µm is compared to the $\delta^{18}O$ measured classically within the 250 and 350 µm fraction from Caley et al. (2011). The dashed line corresponds to the line 1:1.

Regenberg et al. (2014) defines a critical depth threshold above which the preservation is good enough to ensure that Mg/Ca is not noticeably affected by dissolution. This corresponds to water depths about 1–1.5 km shallower than local calcite-saturation horizon. We may hypothesize that this threshold is also valid for the preservation of clumped isotopes. Our MD96-2048 site is above this threshold, suggesting that paleotemperature reconstructions are not affected by dissolution. In addition, the branched and isoprenoid tetraether (BIT) index show very low values over the last 0.8 Ma (Caley et al., 2011), suggesting small input of organic matter from the Limpopo River into the sediment. This condition ensures a good preservation of the shells and a low probability of supra-lysoclinal dissolution resulting from the oxidation of organic matter and the release of CO_2. Finally, we check the preservation of foraminifer tests with scanning electron microscopy (SEM) observations (Fig. 7). We have selected five stratigraphic levels and several specimens of *G. ruber* s. s. per level. We have crushed a few foraminifera and cleaned them with water to remove the large particles find at the surface and inside the tests. Dissolution on foraminifera is usually highlighted by smoothed test surface, absence of spines, denudated spine bases and ridges, and asymmetric pores (Dittert and Henrich, 2000; De Villiers, 2005; Tachikawa et al., 2008; Iwasaki et al., 2015).

The stratigraphic levels selected are:

(i) The core top, as reference for which we expect no or limited dissolution; Fig. 7, first line:

The SEM pictures show no evidence of dissolution at the core top level. These pictures show the preservation of spines, spine bases, ridges, interpore area and rounded pores. The Mg-rich layers inside the

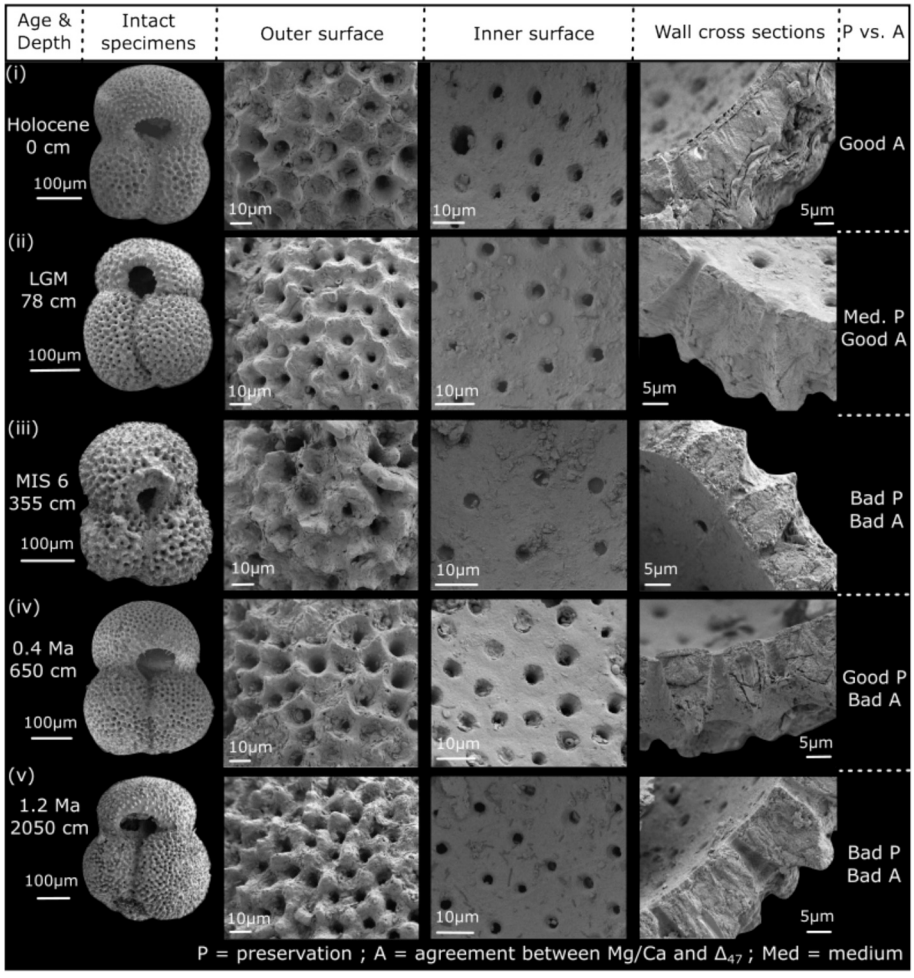

Fig. 7. SEM pictures showing the preservation of the *G. ruber* s. s. shells from 5 different stratigraphic levels compared to the core top. The lines correspond to the samples ranging in stratigraphic order. The columns correspond, respectively, to the age and depth of the samples, the SEM pictures of the intact specimens, the outer and inner surface and the wall cross sections. The last column is the preservation (good, medium and poor) compared to the core top considered as the reference, and the agreement between Mg/Ca-SST and Δ_{47}-SST (good or bad). Horizontal white bars correspond to the scale.

chambers, which we would expect to be dissolved preferentially, is also very well preserved. We can also note the absence of recrystallisation at the surface of the foraminiferal tests.

(ii) The last glacial maximum (LGM) sample (at 78 m); Fig. 7, second line:

The SEM pictures show a medium preservation compared to the core top, with more rounded ridges, slightly clogged pores and slightly eroded Mg-rich layers inside the chambers. Interestingly, this sample was selected to observe potential differences between an interglacial and a glacial period, when Mg/Ca and Δ_{47} are in good agreement.

(iii) The potential outlier at the MIS 6 (at 0.146 Ma; 355 m); Fig. 7, third line:

This sample corresponds to the only datapoint recording large difference between Mg/Ca-SST and Δ_{47}-SST over the last 0.4 Ma. The SEM pictures show that the surface of the tests is smoothed, and the pores are asymmetric, indicating poor preservation of the foraminifer. This poor preservation is also highlighted by recrystallisation at the surface and within the Mg-rich layer in the chambers and clogged pores. Poor preservation of the foraminiferal tests can explain the unrealistic Δ_{47}-SST estimated at this sample depth.

(iv) The first sample dating at 0.4 Ma, recording a significant difference between Mg/Ca-SST and Δ_{47}-SST (at 650 m); Fig. 7, fourth line:

The chamber wall is preserved as well as the core top wall with preservation of spines, spine bases, ridges, interpore area and rounded pores. The Mg-rich layers inside the chambers is also well preserved, implying limited or no effects of diagenetic processes and dissolution. Interestingly, this sample record good preservation but a poor agreement between the Mg/Ca-SST and Δ_{47}-SST.

(v) An old sample (at 1.205 Ma), also recording an offset between Mg/Ca and Δ_{47} (at 1.2 Ma; 2050 m); Fig. 7, fifth line:

The SEM pictures show a bad preservation compared to the core top with rounded ridges, slightly clogged and small pores and eroded Mg-rich layers inside the chambers. The pores are also asymmetric. All these observations point toward poor preservation of the shells.

Digenetic processes can explain some, but not all, of the disagreement between the Mg/Ca and Δ_{47} thermometers. The potential outlier from MIS 6 can be entirely explained by poor shell preservation, conservatively affecting isotopic methods. However, the systematic shift up to 0.4 Ma cannot be entirely explained by preservation issues because the 0.4 Ma sample records very similar preservation to the sample from the upper part of the core. Also, micro-recrystallization cannot be completely excluded as a potential explanation or part of explanation in the difference between the two thermometers. However, it is important to note that further studies on the effect of foraminiferal micro-recrystallization on Δ_{47} are needed to better constrain and quantify this effect in temperature reconstructions.

4.3. Calibration issues

4.3.1. Mg/Ca corrected calibrations

Mg/Ca thermometry requires corrections due to its dependence on secondary parameters other than temperatures alone, such as salinity, pH (estimated from ice core CO_2 reconstruction and before 0.8 Ma from boron isotopic measurements) and the Mg/Ca of seawater (Mg/Ca_{sw}; see methods). Peral et al. (2018) showed that on core top samples, correction for salinity and pH allows reconciliation between these two thermometers. However, can these corrections explain the differences with Δ_{47}-SST?

The Mg/Ca-SST corrected using the equation of Gray and Evans (2019) for global salinity and pH effects in *G. ruber* s. s. (Fig. 8.b; Method 2), show a poor agreement (far from the line 1:1) with Δ_{47}-SST. These estimated Mg/Ca temperatures are similar to those obtained following the Mg/Ca-temperature conversion from Method 1 (Fig. 8b). No significant differences are observed either with Method 3 (Fig. 8.c), when using estimated local salinity G-IG variations rather than using an estimated global salinity from open ocean conditions, as used by Gray and Evans (2019). In addition, the salinity correction presents a large uncertainty, as salinity changes are not well constrained. However, no other methods are available on the studied core. We also added a pH correction before and after 0.8 Ma (see methodology – Method 3).

We also investigated the effect of Mg/Ca_{sw} on Mg/Ca-SST (see methodology, Method 4). The Δ_{47}-SST compared to the Mg/Ca-SST corrected for local salinity, global pH and Mg/Ca_{sw} do not show a better agreement (far from the line 1:1; Fig. 8.d) than compared to the classical Mg/Ca equation (Methods 1, 2 and 3). However, the difference between Mg/Ca-SST and Δ_{47}-SST is larger for old time periods (Fig. 8.d). Mg/Ca-Δ_{47} discrepancy is therefore not eliminated by correcting the Mg/Ca record for salinity, pH and Mg/Ca of the seawater effects (Fig. 8).

It should be noted that the similarity between the Mg/Ca-SST values obtained using method 1 (Anand et al., 2003) and the corrected values from methods 2, 3, and 4 is likely due to the higher Mg/Ca temperature sensitivity (~9%/°C) in the approach used by Anand et al. (2003). Indeed, this approach implicitly incorporates the effects of pH, as pH and temperature vary together. However, since temperature is not the only control on Mg/Ca and is not the only factor influencing pH in the past, using the equation from Anand et al. (2003) often leads to inaccurate results in certain ocean regions (see, for example, Fig. S5 on the Last Glacial Maximum in Gray and Evans, 2019).

The comparison between Mg/Ca-derived SSTs from G. ruber and T. sacculifer, showing only a few minor discrepancies, may point to uncertainties in how past pH is estimated—particularly across varying temporal and spatial scales. Similarly, the few differences observed over time older than 0.4 Ma in the comparison between Δ_{47}-derived SSTs from *G. ruber* and Mg/Ca-derived SSTs from *T. sacculifer* may also be influenced by spatial and temporal variations in salinity. Indeed, the additional corrections on the Mg/Ca-SST method, which are made necessary due to the dependance of Mg/Ca to secondary factors, can vary spatially, specifically in costal environments. We therefore investigate the potential role of strong local variations in the Mg/Ca-derived estimation. It is important to note that the salinity is the secondary parameter that has the strongest influence on Mg/Ca after the temperature, so seasonal and spatial variations of present-day salinity are more crucial to take into account. Salinity changes of 0.04 unit maximum between seasons or 0.05 unit between the surface (1.25 m depth) and the sub-surface (95 m depth). These data are based on the World Ocean Atlas (Locarnini et al., 2024; Reagan et al., 2024) for both temperature and salinity (Table 1). The present day seasonal and vertical local variations at our site are therefore quite small. As a comparison, to compensate for the LGM pH change relative to the modern in the entire ocean, a salinity change of 3–4 PSU would be required, which almost no region experienced.

Today, the area with the strongest local variations is the Bay of Bengal. The pH is estimated to locally change by a maximum of 0.1 and salinity by 7 units (Kumar et al., 2023). The current local variations of Mg/Ca_{sw} in the ocean are estimated to change by 0.2 mol:mol (Lebrato et al., 2020). Here, we estimate the temperature from local salinity and pH changes based on these data (Table 2), resulting in a 4.1 °C change for a maximum 7 units salinity change, a 0.3 °C change for a 0.2 Mg/Ca_{sw} change and a 1.4 °C change for a 0.1 pH change. After compensation effect, a total and maximum value of 3 °C (additions of the temperature differences from the three variable parameters in Table 2) can be explained by strong local changes in salinity, pH and Mg/Ca_{sw}. Thus, assuming the strongest possible local variations of secondary

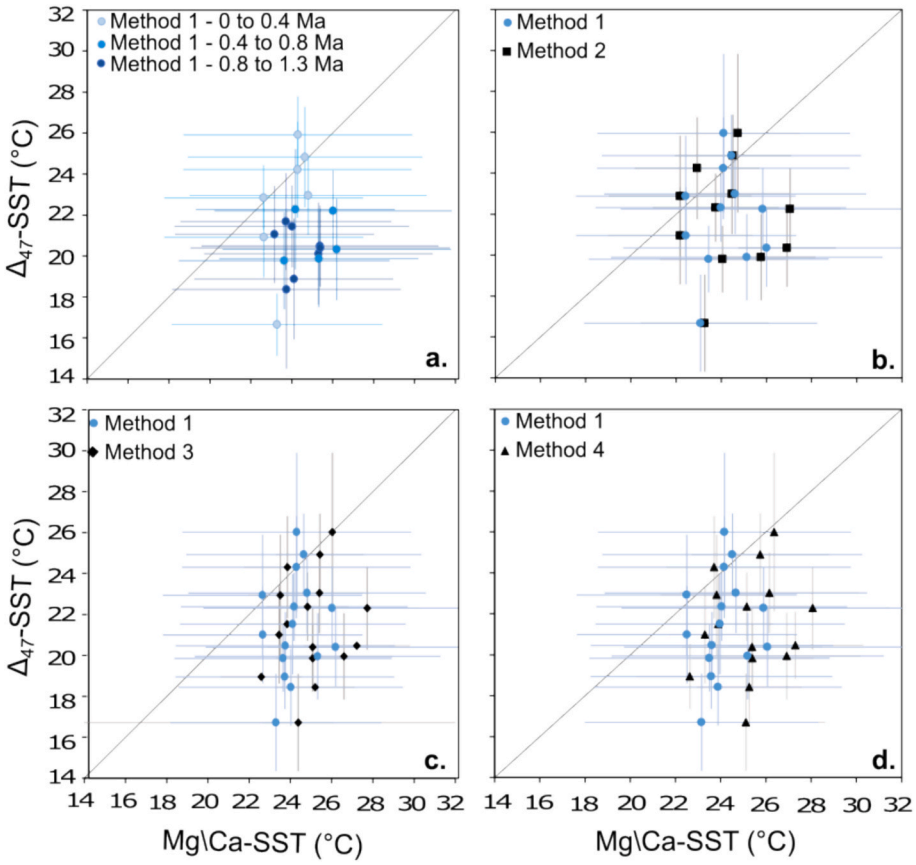

Fig. 8. Comparison of Δ_{47}-SST with the different methods to reconstruct Mg/Ca-SST. Panel (a) corresponds to the Mg/Ca-SST converted with Method 1 (Anand et al., 2003) and compared to Δ_{47}-SST. Light blue corresponds to the SST over the last 0.4 Ma, medium blue from 0.4 to 0.8 Ma and dark blue from 0.8 to 1.2 Ma. Panel (b) corresponds to the comparison between Δ_{47}-SST and Mg/Ca-SST using Method 1 (light blue circles; Anand et al., 2003) and using Method 2 (black squares; Gray and Evans, 2019 over the last 0.8 Ma). Panel (c) corresponds to the comparison between Δ_{47}-SST and Mg/Ca-SST using Method 1 (light blue circles; Anand et al., 2003) and using Method 3 (black diamonds; Gray and Evans, 2019 using local salinity and global pH from 0.8 Ma to 1.25 Ma). Panel (d) corresponds to the comparison between Δ_{47}-SST and Mg/Ca-SST using Method 1 (light blue circles; Anand et al., 2003) and using Method 4 (black triangles; Gray and Evans, 2019 modified with local salinity and global pH and Mg/Ca_{sw} from 0.8 Ma to 1.25 Ma). Uncertainties are at 2 sigma.

parameters, the Mg/Ca-SST change cannot compensate for up to 8 °C difference between Mg/Ca- (Method 4) and Δ_{47}-SST. In addition, our working area is not known to experience such extreme local variations. The core site is located close to the Limpopo delta. Variations in its discharge over time may have impacted salinity or transported elements that could bias the geochemical signals. However, XRF data from the MD96-2048 core suggest a long-term aridification in the Limpopo catchment between approximately 1 and 0.6 million years ago (Caley et al., 2018), indicating reduced freshwater input and a potential increase in salinity, which would induce apparently cooler Mg/Ca-temperature estimates (Table 2). This observation contrasts with expectations, as the two temperature proxies began to diverge around 0.4 Ma: reduction of the river discharge would result on lower SST estimated in Mg/Ca, and reduce the differences with the Δ_{47}. In addition, the Branched and Isoprenoid Tetraether (BIT) index over the past 0.8 Ma shows consistently low values, suggesting that fluvial influence at the core site is limited (Caley et al., 2011). Similarly, low pollen percentages were found (Dupont et al., 2011). Together, these findings suggest that the contribution of terrestrial soil material in the studied core is weak over time, and that oceanic parameters (SST, SSS), reconstructed from MD96-2048 core primarily reflect changes in the upstream dynamics of the Agulhas Current rather than fluctuations in coastal waters. Local changes due to costal position of the core is unlikely to explain the differences between Δ_{47}-SST and Mg/Ca-SST. However, despite the difficulties in accurately reconstructing these local hydrographic variations in the past, it would be important to take them into account as much as possible and to develop, more particularly, new methods to precisely reconstruct the salinity, the parameter which has the strongest effect in Mg/Ca-SST reconstructions after the temperature (Table 2). In summary, as we found it unlikely that local variations in pH, salinity and Mg/Ca_{sw} alone can explain the important differences between SST from Mg/Ca-*G. ruber*, Mg/Ca-*T. sacculifer* and Δ_{47}-*G. ruber* prior to 0.4 Ma, there is a need to look for other mechanisms.

4.3.2. Δ_{47} foraminiferal calibrations

Even though recent clumped isotope calibrations on planktonic foraminifera are robust (Peral et al., 2018, 2020; Meinicke et al., 2020,2021), the estimations of the temperature of foraminiferal calcification are quite challenging. We used the recent study (Daëron and Gray, 2023) which re-estimated temperature of foraminiferal calcification of the pre-existing calibrations, yielding a Δ_{47}-T relationship statistically indistinguishable from that in many other biogenic and inorganic calibrations (Daëron and Vermeesch, 2024). Temperatures reconstructed using this updated calibration are colder than those using the previously published equations (Fig. 9). However, a similar result with colder Δ_{47}-SST than Mg/Ca-SST is observed using Peral et al. (2020) and Daëron and Gray (2023) calibrations. The slightly higher temperatures reconstructed using Meinicke et al. (2021) can be explained as this calibration also includes benthic foraminifera from Piasecki et al. (2019), which is not ideal (Daëron and Gray, 2023). Furthermore, applying the calibration from Meinicke et al. (2021) results in overly warm temperature estimates for the recent time interval

Table 1
Modern temperature and salinity from World Ocean Atlas at our site (Locarnini et al., 2024; Reagan et al., 2024).

Methods	Values	SE (°C)	References	Water depth	Season
Temperature (°C)	24,9	2,2	Locarnini et al., 2018	Surface	Annual
	21	1,7	Locarnini et al., 2018	Sub-surface	Annual
	22,8	0,9	Locarnini et al., 2018	Surface	Summer NH
	27,1	1,23	Locarnini et al., 2018	Surface	Winter NH
	25,1	1,55	Locarnini et al., 2018	Surface	Spring NH
	24,8	1,3	Locarnini et al., 2018	Surface	Autonm NH
Salinity	35.32	0.15	Reagan et al., 2024	Surface	Annual
	35.37	0.08	Reagan et al., 2024	Sub-surface	Annual
	35.31	0.13	Reagan et al., 2024	Surface	Winter
	35.34	0.18	Reagan et al., 2024	Surface	Summer
	35.3	0.08	Reagan et al., 2024	Surface	Autumn
	35.34	0.03	Reagan et al., 2024	Surface	Spring

Table 2
Test of Mg/Ca sensitivity to strong local pH, salinity and Mg/Ca_{sw} changes. The pH, salinity and Mg/Ca_{sw} vary based on the strongest local variations in the Indian Ocean (italic values). The differences correspond to the difference in temperatures estimated with highest and lowest local variations of the variable parameters (pH, salinity, Mg/Ca of seawater). For the first two lines (pH varies and salinity varies). The Mg/Ca-SST are calculated using Method 3 and the last line, using Method 4.

Variable parameters	*pH*	*Salinity*	*Mg/Ca_{sw}*	*Mg/Ca*	*T (°C)*	*Differences*
pH	**8.1**	35		4	23.7	−1.4
range	***8.2***	35		4	25.1	
Salinity	8.1	**32**		4	25.4	4.1
range	8.1	***39***		4	21.3	
Mg/Ca_{sw}	8.1	35	**5.0**	4	25.3	0.3
range	8.1	35	***5.2***	4	25.0	

Total temperature explained by strong local changes = 3 °C.

and persistently cold estimates for the older interval (Fig. 9). All SST values derived from the three Δ_{47}-SST calibrations are comparable within their respective uncertainties, differing by an average of only 1.4 °C. As a result, issues with Δ_{47} calibration are unlikely to account for the differences between Δ_{47}-SST and Mg/Ca-SST, which can still reach up to 4.7 °C when using the calibration from Meinicke et al. (2021) (Fig. 9).

4.4. Alternative, untested hypotheses

The species *T. sacculifer* is ideally suited for Mg/Ca SST reconstructions (Allen et al., 2016; Gray and Evans, 2019; Haynes et al., 2023). Thus, the comparison between Mg/Ca on *T. sacculifer* and on *G. ruber* would help determine whether the Mg/Ca-SST on *G. ruber* is influenced by variable DIC and pH. In Fig. 5.a, the comparison shows a general good agreement. However, for two samples (over the seven measurements) differences larger than error bars occur and for different time interval (before and after 0.4 Ma). As pH might have preferentially biased Mg/Ca *G. ruber*, these differences could be due to the absence of appropriate pH data at the study site or due to difference in living depth

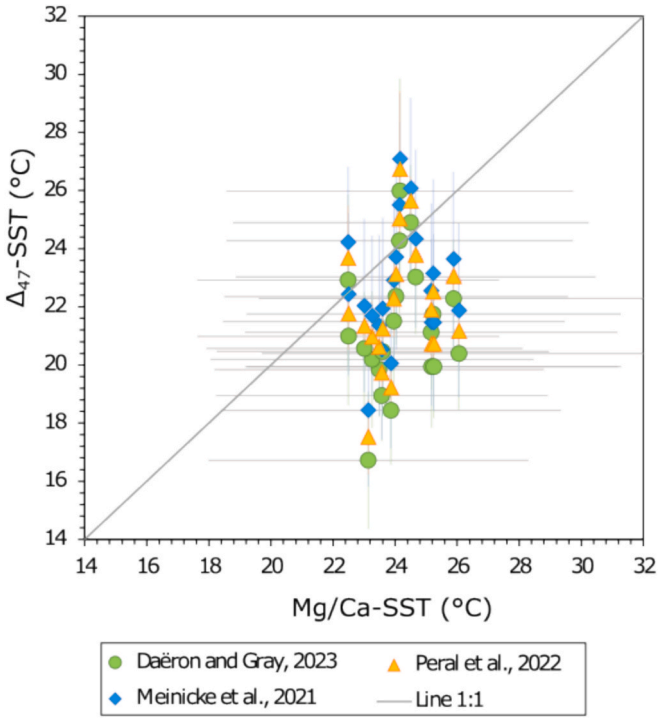

Fig. 9. Comparison of Mg/Ca-SST with the different foraminiferal based calibrations to reconstruct Δ_{47}-SST. The Mg/Ca-SST converted with Method 1 (Anand et al., 2003) is compared to Δ_{47}-SST using Daëron and Gray (2023) calibration (green dots), Meinicke et al. (2021) calibration (blue diamonds) and Peral et al. (2022) calibration (orange triangle). Uncertainties are at 2 sigma.

and seasonality between the two species. The difference can be up to 4 °C (Fig. 5). Today the largest difference in seasonality at the surface is also 4 °C (22.8 ± 0.9 °C during winter and 27.1 ± 1.2 °C during summer). However, in the core top sample, the Mg/Ca-SST of *T. sacculifer* and of *G. ruber* are indistinguishable; i.e. 23.5 ± 1.5 °C and 23.0 ± 2.8 °C, respectively (using species specific equations of Gray and Evans (2019)). Additional measurements and datasets would be needed to investigated the slight disagreement between the 2 species.

The comparison between Mg/Ca-SST measured on *T. sacculifer* and Δ_{47}-SST measured on *G. ruber* show colder Δ_{47}-SST after 0.4 Ma (Fig. 5. b) as shown by comparing both thermometers only on *G. ruber* (Fig. 4). These differences can be due to a change in the relationship between Mg/Ca and seawater temperature, salinity, pH and Mg/Ca. This relation may not be linear in the past. For example, low Mg/Ca_{sw} values, close to Paleocene water carbonate chemistry, can limit the effect of pH in the Mg/Ca measurements (Haynes et al., 2023). In our case, changes in surface water chemistry around 0.4 Ma, compared to current conditions, were almost certainly of a smaller magnitude than the changes that prevailed during the Paleocene. A potential change around 0.4 Ma is unlikely but we cannot fully eliminate this hypothesis.

Another explanation is an issue on clumped isotope method, such as a change in the biomineralization processes, or a secondary effect of seawater pH or a still unknown effect. Planktonic foraminiferal calibrations in Δ_{47} (Peral et al., 2018, 2020; Meinicke et al., 2020,2021) agree with the other calibrations performed on several different carbonates (Anderson et al., 2021; Daëron and Gray, 2023; Daëron and Vermeesch, 2024; Marchegiano et al., 2024), which suggest that the same relationship between foraminiferal Δ_{47} and temperature holds true for both bio- and inorganic carbonates. A biomineralization bias affecting clumped isotopes is therefore unlikely. It should be noted that the Δ_{47}-SST decreases significantly prior to 0.4 Ma, while the Mg/Ca-SST is constant (Fig. 3). Northward shifts of the subtropical front were

documented in this area around 0.4 Ma (Bard and Rickaby, 2009). But our study site is too far to the North to be affected by the subtropical front and a decrease of temperatures. On the contrary, our site could be influenced by the build-up of heat from the return flow of the Agulhas current associated to the latitudinal contraction of subtropical gyres (Sijp and England, 2008; Caley et al., 2011). Furthermore, the planktonic foraminiferal $\delta^{18}O$ curve displays glacial-interglacial variations comparable to the $\delta^{18}O$ stack of Lisiecki and Raymo (2005) (Caley et al., 2011). Since there is no noticeable change in foraminiferal $\delta^{18}O$ around 0.4 Ma, if the important change in temperature suggested by the Δ_{47}-SST were real, a very large modification in $\delta^{18}O_{sw}$ would be required to "compensate" for the temperature effect on the foraminiferal $\delta^{18}O$ and thus explain the lack of variation in this record. By combining foraminiferal $\delta^{18}O$ and Δ_{47}-SST, we calculate an amplitude of approximately 1 ‰ in the $\delta^{18}O_{sw}$ shift around 0.4 Ma (Fig. 10). It seems unlikely that this change could be linked to variations in salinity as there are no other evidence and studies suggesting a significant shift in salinity at this period. As mentioned previously, there are no variations in river discharges, as supported by the XRF data, BIT index, and pollen content (Dupont et al., 2011; Caley et al., 2011). A global salinity change in the Indian Ocean at 400 ka is also unlikely as concluded by Nuber et al. (2023). Since there is no objective evidence supporting the existence of a massive change in $\delta^{18}O_{sw}$ around 0.4 Ma, the significant SST change shown by the Δ_{47} measurements should be seriously questioned. Many well-known biases (e.g., salinity, pH, diagenesis, etc.) have been examined in numerous studies and in this study, all of which concluded that they do not affect Δ_{47} (Tripati et al., 2010; Grauel et al., 2013; Breitenbach et al., 2018; Peral et al., 2018, 2020; Meinicke et al., 2020). There is also no oceanographic explanation nor any potential suggestion regarding chemical/physical mechanisms that could explain the odd shift observed around 0.4 Ma in Δ_{47}-SST. As a result, our findings are puzzling and temperatures estimated from clumped isotopes are not supported by climatic context. Therefore, the Mg/Ca-SST are consistent while Δ_{47}-SST are probably wrong and affected by secondary effects. Further investigations into the Δ_{47} method applied to planktonic foraminifera are necessary.

In the future, additional datasets comparing the two thermometers are needed to confirm the offset and define whether it is constant, global or regional. This would also help to better define a potential process affecting Δ_{47} or whether a combination of the multiple explanations presented in this study can also explain the offset. Based on a larger dataset, a more concrete explanation may therefore be determined allowing the reconstruction of accurate high-resolution SST reconstructions, therefore improving our understanding of past climate dynamic.

5. Conclusions

In this study, we investigated the offset between foraminiferal Mg/Ca and Δ_{47}, yielding substantially colder Δ_{47}-SST than Mg/Ca-SST before 0.4 Ma. Scanning Electron Microscope pictures allow the investigation of preservation states by tracking dissolution or recrystallisation of the tests. Here, bad preservation can explain the unrealistic cold MIS 6 Δ_{47}-SST but cannot fully explain the systematic offset between the two thermometers from 1.25 to 0.4 Ma, as the sample at 0.4 Ma show a good preservation, similar to the core-top preservation. The corrections of Mg/Ca-SST for seawater salinity, pH or Mg/Ca do not explain the differences with the Δ_{47}-SST. Likewise, taking into account potential strong local variations in these secondary parameters cannot explain the differences. The offsets can neither be explained by potential differences arising from the use of different Δ_{47} calibrations. The Δ_{47}-SST cooling around 0.4 Ma would be explain by a change in seawater $\delta^{18}O$ of approximative 1 ‰ around 0.4 Ma, however, this change is quite unlikely as no evidences have been found in previous studies, such as change in freshwater input from the river. As Δ_{47}-SST are inconsistent with the climatic context, we propose that Δ_{47}-SST are affected by an unknown process. A combination of the multiple explanations presented in this study can also explain the offset. Additional datasets comparing Mg/Ca and Δ_{47} are needed to better constrain limitations of both proxies. The offset can have crucial implications for past SST reconstructions and paleoceanography.

Data availability

Clumped isotope data is available through EarthChem at https://doi.org/10.60520/IEDA/113853. Mg/Ca data on *T. sacculifer* is available through Pangaea at https://doi.pangaea.de/10.1594/PANGAEA.983363.

CRediT authorship contribution statement

Marion Peral: Writing – original draft, Visualization, Validation, Investigation, Formal analysis, Data curation, Conceptualization. **Thibaut Caley:** Writing – original draft, Validation, Supervision, Investigation, Formal analysis, Conceptualization. **Bruno Malaizé:** Writing – original draft, Validation, Supervision, Investigation, Formal analysis, Conceptualization. **Thomas Extier:** Writing – review & editing, Validation, Investigation, Formal analysis, Conceptualization. **Linda Rossignol:** Writing – review & editing, Validation, Investigation, Formal analysis. **Héloïse Barathieu:** Writing – review & editing, Validation, Investigation, Formal analysis. **Émilie Dassié:** Writing – review & editing, Validation, Supervision, Investigation, Formal analysis. **Franck Bassinot:** Writing – review & editing, Supervision, Investigation, Funding acquisition. **Dominique Blamart:** Writing – review & editing,

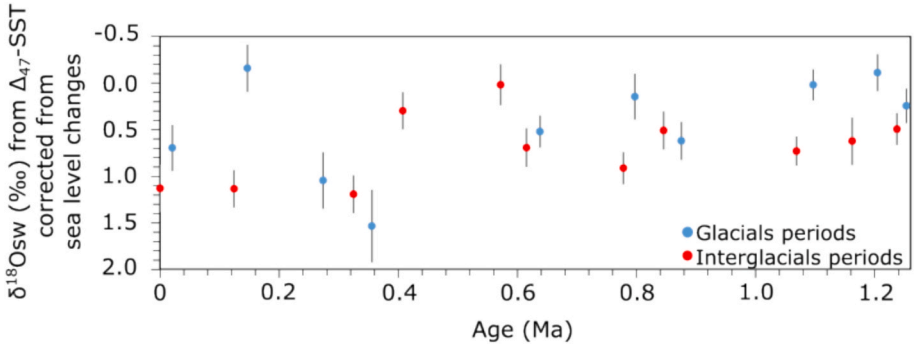

Fig. 10. $\delta^{18}Osw$ **reconstructions based on** Δ_{47}**-SST.** The $\delta^{18}Osw$ show lower average values (about 1 ‰ difference) before 0.4 Ma then after. The $\delta^{18}Osw$ is corrected for sea level changes and should reflect sea surface salinity changes. The glacial periods are in blue, the interglacial in red. The uncertainties are presented at 2 sigma.

Validation, Supervision, Funding acquisition, Formal analysis. **Mathieu Daëron:** Writing – review & editing, Validation, Supervision, Funding acquisition, Formal analysis.

Declaration of competing interest

The authors declare that they have no known competing financial interests or personal relationships that could have appeared to influence the work reported in this paper.

Acknowledgements

Core MD96-2048 was collected during the MOZAPHAR cruise of the RV Marion Dufresne, supported by the French agencies Ministère de l'Education Nationale de la Recherche et de la Technologie, Centre National de la Recherche Scientifique (CNRS), and Institut Paul Emile Victor (IPEV). MP thanks, for financial support, the CEA during her PhD fellowship and Phillipe Claeys from the VUBrussels during her post-doctoral position. MP and LR thank both, the biodiversity platform of EPOC laboratory from the University of Bordeaux and the Bordeaux Imaging Center for the support with the SEM instruments. The authors thank the editor and the reviewers for their time spent reviewing the manuscript and for their valuable comments and suggestions, which helped us improve the manuscript.

References

Allen, K.A., Hönisch, B., Eggins, S.M., Haynes, L.L., Rosenthal, Y., Yu, J., 2016. Trace element proxies for surface ocean conditions: a synthesis of culture calibrations with planktic foraminifera. Geochim. Cosmochim. Acta 193, 197–221.

Anand, P., Elderfield, H., Conte, M.H., 2003. Calibration of Mg/Ca thermometry in planktonic foraminifera from a sediment trap time series. Paleoceanography 18 (2).

Anderson, N.T., Kelson, J.R., Kele, S., Daëron, M., Bonifacie, M., Horita, J., Bergmann, K. D., 2021. A unified clumped isotope thermometer calibration (0.5–1,100 C) using carbonate-based standardization. Geophys. Res. Lett. 48 (7).

Bard, E., Rickaby, R.E., 2009. Migration of the subtropical front as a modulator of glacial climate. Nature 460 (7253), 380–383.

Barker, S., Greaves, M., Elderfield, H., 2003. A study of cleaning procedures used for foraminiferal Mg/Ca paleothermometry. Geochemistry. Geophys. Geosyst. 4, 1–20.

Bernasconi, S.M., Daëron, M., Bergmann, K.D., Bonifacie, M., Meckler, A.N., Affek, H.P., Anderson, N., Bajnai, D., Barkan, E., Beverly, E., Blamart, D., Burgener, L., Calmels, D., Chaduteau, C., Clog, M., Davidheiser-Kroll, B., Davies, A., Dux, F., Eiler, J., Elliott, B., Fetrow, A., Fiebig, J., Goldberg, S., Hermoso, M., Huntington, K. W., Hyland, E., Ingalls, M., Jaggi, M., John, C.J., Jost, A.B., Katz, S., Kelson, J., Kluge, T., Kocken, I.J., Laskar, A., Leutert, T.J., Liang, D., Lucarelli, J., Mackey, T.J., Mangenot, X., Meinicke, N., Modestou, S.E., Mueller, I.A., Murray, S., Neary, A., Packard, N., Passey, B.H., Pelletier, E., Petersen, S., Piasecki, A., Schauer, A., Snell, K.E., Swart, P.K., Tripati, A., Upadhyay, D., Vennemann, T., Winkelstern, I., Yarian, D., Yoshida, N., Zhang, N., Ziegler, M., 2021. InterCarb: a community effort to improve inter-laboratory standardization of the carbonate clumped isotope thermometer using carbonate standards. Geochem. Geophys. Geosyst. 22 (5).

Bintanja, R., Van de Wal, R.S.W., 2008. North American ice-sheet dynamics and the onset of 100,000-year glacial cycles. Nature 454 (7206), 869–872.

Brand, W.A., Assonov, S.S., Coplen, T.B., 2010. Correction for the 17O interference in δ(13C) measurements when analyzing CO2 with stable isotope mass spectrometry (IUPAC Technical Report). Pure Appl. Chem. 82, 1719–1733.

Breitenbach, S.F.M., Mleneck-Vautravers, M.J., Grauel, A.-L., Lo, L., Bernasconi, S.M., Müller, I.A., Rolfe, J., Greaves, M., Hodell, D.A., 2018. Coupled Mg/Ca and clumped isotope analyses of foraminifera provide consis- tent water temperatures. Geochim. Cosmochim. Acta 236, 283–296.

Caley, T., Kim, J.H., Malaizé, B., Giraudeau, J., Laepple, T., Caillon, N., Sinninghe Damsté, J.S., 2011. High-latitude obliquity as a dominant forcing in the Agulhas current system. Clim. Past 7 (4), 1285–1296.

Caley, T., Extier, T., Collins, J.A., Schefuß, E., Dupont, L., Malaizé, B., Giraudeau, J., 2018. A two-million-year-long hydroclimatic context for hominin evolution in southeastern Africa. Nature 560 (7716), 76–79.

Chalk, T.B., Hain, M.P., Foster, G.L., Rohling, E.J., Sexton, P.F., Badger, M.P., Wilson, P. A., 2017. Causes of ice age intensification across the Mid-Pleistocene transition. Proc. Natl. Acad. Sci. 114 (50), 13114–13119.

Daëron, M., Blamart, D., Peral, M., Affek, H.P., 2016. Absolute isotopic abundance ratios and the accuracy of Δ47 measurements. Chem. Geol. 442, 83–96.

Daëron, M., 2021. Full propagation of analytical uncertainties in Δ47 measurements. Geochem. Geophys. Geosyst. 22 (5).

Daëron, M., Gray, W.R., 2023. Revisiting oxygen-18 and clumped isotopes in planktic and benthic foraminifera. Paleoceanogr. Paleoclimatol. 38 (10).

Daëron, M., Vermeesch, P., 2024. Omnivariant generalized least squares regression: theory, geochronological applications, and making the case for reconciled Δ47 calibrations. Chem. Geol. 647, 121881.

De Villiers, S., 2005. Foraminiferal shell-weight evidence for sedimentary calcite dissolution above the lysocline. Deep Sea Res. Part I 52 (5), 671–680.

De Vleeschouwer, D., Peral, M., Marchegiano, M., Füllberg, A., Meinicke, N., Pälike, H., Claeys, P., 2022. Plio-Pleistocene Perth Basin water temperatures and Leeuwin current dynamics (Indian Ocean) derived from oxygen and clumped-isotope paleothermometry. Clim. Past 18 (5), 1231–1253.

Dittert, N., Henrich, R., 2000. Carbonate dissolution in the South Atlantic Ocean: evidence from ultrastructure breakdown in Globigerina bulloides. Deep Sea Res. Part I 47 (4), 603–620.

Dupont, L.M., Caley, T., Kim, J.H., Castañeda, I., Malaizé, B., Giraudeau, J., 2011. Glacial-interglacial vegetation dynamics in South Eastern Africa coupled to sea surface temperature variations in the Western Indian Ocean. Clim. Past 7 (4), 1209–1224.

Elderfield, H., Vautravers, M., Cooper, M., 2002. The relationship between shell size and Mg/Ca, Sr/Ca, δ18O, and δ13C of species of planktonic foraminifera. Geochem. Geophys. Geosyst. 3 (8), 1–13.

Elderfield, H., Yu, J., Anand, P., Kiefer, T., Nyland, B., 2006. Calibrations for benthic foraminiferal Mg/Ca paleothermometry and the carbonate ion hypothesis. Earth Planet. Sci. Lett. 250, 633–649.

Evans, D., Müller, W., 2012. Deep time foraminifera Mg/Ca paleothermometry: nonlinear correction for secular change in seawater Mg/Ca. Paleoceanography 27 (4).

Evans, D., Brierley, C., Raymo, M.E., Erez, J., Müller, W., 2016. Planktic foraminifera shell chemistry response to seawater chemistry: Pliocene-Pleistocene seawater Mg/Ca, temperature and sea level change. Earth Planet. Sci. Lett. 438, 139–148.

Fiebig, J., Bernecker, M., Meijer, N., Methner, K., Staudigel, P.T., Davies, A.J., Bayarjargal, L., Spahr, D., Winkler, B., Hofmann, S., Granzin, M., Petersen, S.V., 2024. Carbonate clumped isotope values compromised by nitrate-derived NO2 interferent. Chem. Geol. 670, 122382.

Friedrich, O., Schiebel, R., Wilson, P.A., Weldeab, S., Beer, C.J., Cooper, M.J., Fiebig, J., 2012. Influence of test size, water depth, and ecology on Mg/Ca, Sr/Ca, δ18O and δ13C in nine modern species of planktic foraminifers. Earth Planet. Sci. Lett. 319, 133–145.

Garcia, H. E., Weathers, K. W., Paver, C. R., Smolyar, I., Boyer, T. P., Locarnini, M. M., ... Seidov, D., 2019. World Ocean Atlas 2018, Volume 3: Dissolved Oxygen, Apparent Oxygen Utilization, and Dissolved Oxygen Saturation.

Ghosh, P., Eiler, J., Campana, S.E., Feeney, R.F., 2007. Calibration of the carbonate 'clumped isotope'paleothermometer for otoliths. Geochim. Cosmochim. Acta 71 (11), 2736–2744.

Gothmann, A.M., Stolarski, J., Adkins, J.F., Schoene, B., Dennis, K.J., Schrag, D.P., Bender, M.L., 2015. Fossil corals as an archive of secular variations in seawater chemistry since the Mesozoic. Geochim. Cosmochim. Acta 160, 188–208.

Grauel, A.L., Schmid, T.W., Hu, B., Bergami, C., Capotondi, L., Zhou, L., Bernasconi, S.M., 2013. Calibration and application of the "clumped isotope" thermometer to foraminifera for high-resolution climate reconstructions. Geochim. Cosmochim. Acta 108, 125–140.

Gray, W.R., Weldeab, S., Lea, D.W., Rosenthal, Y., Gruber, N., Donner, B., Fischer, G., 2018. The effects of temperature, salinity, and the carbonate system on Mg/Ca in Globigerinoides ruber (white): a global sediment trap calibration. Earth Planet. Sci. Lett. 482, 607–620.

Gray, W.R., Evans, D., 2019. Nonthermal influences on Mg/Ca in planktonic foraminifera: a review of culture studies and application to the last glacial maximum. Paleoceanogr. Paleoclimatol. 34 (3), 306–315.

Grubbs, F.E., 1969. Procedures for detecting outlying observations in samples. Technometrics 11 (1), 1–21.

Haynes, L.L., Hönisch, B., Holland, K., Eggins, S., Rosenthal, Y., 2023. Calibrating non-thermal effects on planktic foraminiferal Mg/Ca for application across the Cenozoic. Paleoceanogr. Paleoclimatol. 38 (10).

Horita, J., Zimmermann, H., Holland, H.D., 2002. Chemical evolution of seawater during the Phanerozoic: Implications from the record of marine evaporites. Geochim. Cosmochim. Acta 66 (21), 3733–3756.

Iwasaki, S., Kimoto, K., Sasaki, O., Kano, H., Honda, M.C., Okazaki, Y., 2015. Observation of the dissolution process of Globigerina bulloides tests (planktic foraminifera) by X-ray microcomputed tomography. Paleoceanography 30 (4), 317–331.

Kim, S.T., O'Neil, J.R., Hillaire-Marcel, C., Mucci, A., 2007. Oxygen isotope fractionation between synthetic aragonite and water: Influence of temperature and Mg2+ concentration. Geochim. Cosmochim. Acta 71 (19), 4704–4715.

Kısakürek, B., Eisenhauer, A., Böhm, F., Garbe-Schönberg, D., Erez, J., 2008. Controls on shell Mg/Ca and Sr/Ca in cultured planktonic foraminiferan, Globigerinoides ruber (white). Earth Planet. Sci. Lett. 273 (3–4), 260–269.

Kumar, S., Chakraborty, A., Chandrakar, R., Kumar, A., Sadhukhan, B., Roy Chowdhury, R., 2023. Analysis of marine heatwaves over the Bay of Bengal during 1982–2021. Sci. Rep. 13 (1), 14235.

Lamont, T., Roberts, M.J., Barlow, R.G., Morris, T., van den Berg, M.A., 2010. Circulation patterns in the Delagoa Bight, Mozambique, and the influence of deep ocean eddies. Afr. J. Mar. Sci. 32 (3), 553–562.

Lea, D., Mashiotta, T., Spero, H., 1999. Controls on magnesium and strontium uptake in planktonic foraminifera determined by live culturing. Geochim. Cosmochim. Acta 63, 2369–2379.

Lear, C.H., Rosenthal, Y., Slowey, N., 2002. Benthic foraminiferal Mg/Ca-paleothermometry: a revised core-top calibration. Geochim. Cosmochim. Acta 66 (19), 3375–3387.

Leutert, T.J., Auderset, A., Martínez-García, A., Modestou, S., Meckler, A.N., 2020. Coupled Southern Ocean cooling and Antarctic ice sheet expansion during the middle Miocene. Nat. Geosci. 13 (9), 634–639.

Leutert, T.J., Sexton, P.F., Tripati, A., Piasecki, A., Ho, S.L., Meckler, A.N., 2019. Sensitivity of clumped isotope temperatures in fossil benthic and planktic foraminifera to diagenetic alteration. Geochim. Cosmochim. Acta 257, 354–372.

Lisiecki, L.E., Raymo, M.E., 2005. Correction to "a Pliocene-Pleistocene stack of 57 globally distributed benthic d18O records''. Paleoceanography 20, PA2007.

Locarnini, R.A., Mishonov, A.V., Baranova, O.K., Boyer, T.P., Zweng, M.M., Garcia, H.E., Reagan, J.R., Seidov, D., Weathers, K.W., Paver, C.R., Smolyar, I.V., 2019. World Ocean Atlas 2018, Volume 1: Temperature. A. Mishonov, Technical Editor. NOAA Atlas NESDIS 81, 52pp.

Locarnini, R. A., Mishonov, A. V., Baranova, O. K., Reagan, J. R., Boyer, T. P., Seidov, D., Wang, Z., Garcia, H.E., Bouchard, C., Cross, S.L., Paver, C.R., Dukhovskoy, D., 2024. World Ocean Atlas 2023, Volume 1: Temperature. A. Mishonov, Technical Editor. NOAA Atlas NESDIS, pp. 89, 52.

Lutjeharms, J.R., 2006. *The Agulhas Current Retroflection*. Springer, Berlin Heidelberg.

Lüthi, D., Le Floch, M., Bereiter, B., Blunier, T., Barnola, J.M., Siegenthaler, U., Stocker, T.F., 2008. High-resolution carbon dioxide concentration record 650,000–800,000 years before present. Nature 453 (7193), 379–382.

Marchegiano, M., Peral, M., Venderickx, J., Martens, K., García-Alix, A., Snoeck, C., Goderis, S., Claeys, P., 2024. The ostracod clumped-isotope thermometer: a novel tool to accurately quantify continental climate changes. Geophys. Res. Lett. 51 (4).

Marchitto, T.M., Bryan, S.P., Curry, W.B., McCorkle, D.C., 2007. Mg/Ca temperature calibration for the benthic foraminifer Cibicidoides pachyderma. Paleoceanography 22 (1).

Mathien-Blard, E., Bassinot, F., 2009. Salinity bias on the foraminifera Mg/Ca thermometry: correction procedure and implications for past ocean hydrographic reconstructions. Geochem. Geophys. Geosyst. 10.

Meinicke, N., Ho, S.L., Hannisdal, B., Nürnberg, D., Tripati, A., Schiebel, R., Meckler, A. N., 2020. A robust calibration of the clumped isotopes to temperature relationship for foraminifers. Geochim. Cosmochim. Acta 270, 160–183.

Meinicke, N., Reimi, M.A., Ravelo, A.C., Meckler, A.N., 2021. Coupled Mg/Ca and clumped isotope measurements indicate lack of substantial mixed layer cooling in the Western Pacific Warm Pool during the last ~ 5 million years. Paleoceanogr. Paleoclimatol. e2020PA004115.

Mulitza, S., Boltovskoy, D., Donner, B., Meggers, H., Paul, A., Wefer, G., 2003. Temperature: δ18O relationships of planktonic foraminifera collected from surface waters. Palaeogeogr. Palaeoclimatol. Palaeoecol. 202 (1–2), 143–152.

Nuber, S., Rae, J.W., Zhang, X., Andersen, M.B., Dumont, M.D., Mithan, H.T., Barker, S., 2023. Indian Ocean salinity build-up primes deglacial ocean circulation recovery. Nature 617 (7960), 306–311.

Nürnberg, D., Bijma, J., Hemleben, C., 1996. Assessing the reliability of magnesium in foraminiferal calcite as a proxy for water mass temperatures. Geochim. Cosmochim. Acta 60, 803–814.

Peral, M., Daëron, M., Blamart, D., Bassinot, F., Dewilde, F., Smialkowski, N., Isguder, G., Jorissen, F., Kissel, C., Michel, E., Vázquez Riveiros, N., Waelbroeck, C., 2018. ScienceDirect Updated Calibration of the Clumped Isotope Thermometer in Planktonic and Benthic Foraminifera. 239, 1–16.

Peral, M., Blamart, D., Bassinot, F., Daëron, M., Dewilde, F., Rebaubier, H., Nomade, S., Girone, A., Marimo, M., Maiorano, P., Ciaranfi, N., 2020. Changes in temperature and oxygen isotopic composition of Mediterranean water during the Mid-Pleistocene transition in the Montalbano Jonico section (southern Italy) using the clumped-isotope thermometer. Palaeogeogr. Palaeoclimatol. Palaeoecol. 544, 109603.

Peral, M., Bassinot, F., Daëron, M., Blamart, D., Bonnin, J., Jorissen, F., Kissel, C., Michel, E., Waelbroeck, C., Rebaubier, H., Gray, W.R., 2022. On the combination of the planktonic foraminiferal Mg/Ca, clumped (Δ47) and conventional (δ18O) stable isotope paleothermometers in palaeoceanographic studies. Geochim. Cosmochim. Acta 339, 22–34.

Piasecki, A., Bernasconi, S. M., Grauel, A., Hannisdal, B., Ho, S.L., Leutert, T.J., et al., 201 9. Application of clumped isotope thermometry to benthic foraminifera. Geochem. Geophys. Geosyst. 2018GC007961.

Quartly, G.D., Srokosz, M.A., 2004. Eddies in the southern Mozambique Channel. Deep Sea Res. Part II 51 (1–3), 69–83.

Reagan, J.R., Seidov, D., Wang, Z., Dukhovskoy, D., Boyer, T.P., Locarnini, R.A., Baranova, O.K., Mishonov, A.V., Garcia, H.E., Bouchard, C., Cross, S.L., Paver, C.R., 2024. World Ocean Atlas 2023, Volume 2: Salinity. A. Mishonov, Technical Editor, NOAA Atlas NESDIS 90, pp. 52.

Regenberg, M., Regenberg, A., Garbe-Schönberg, D., Lea, D.W., 2014. Global dissolution effects on planktonic foraminiferal Mg/Ca ratios controlled by the calcite-saturation state of bottom waters. Paleoceanography 29 (3), 127–142.

Rosenthal, Y., Boyle, E.A., Slowey, N., 1997. Temperature control on the incorporation of magnesium, strontium, fluorine, and cadmium into benthic foraminiferal shells from Little Bahama Bank: prospects for thermocline paleoceanography. Geochim. Cosmochim. Acta 61 (17), 3633–3643.

Rosenthal, Y., Lear, C.H., Oppo, D.W., Linsley, B.K., 2006. Temperature and carbonate ion effects on Mg/Ca and Sr/Ca ratios in benthic foraminifera: Aragonitic species Hoeglundina elegans. Paleoceanography 21 (1).

Schauble, E.A., Ghosh, P., Eiler, J.M., 2006. Preferential formation of 13C-18O bonds in carbonate minerals, estimated using first-principles lattice dynamics. Geochim. Cosmochim. Acta 70, 2510–2529.

Schiebel, R., Hemleben, C., 2017. Planktic Foraminifers in the Modern Ocean. Springer, Berlin.

Sijp, W.P., England, M.H., 2008. The effect of a northward shift in the southern hemisphere westerlies on the global ocean. Prog. Oceanogr. 79 (1), 1–19.

Staudigel, P.T., John, E.H., Buse, B., Pearson, P.N., Lear, C.H., 2022. Apparent preservation of primary foraminiferal Mg/Ca ratios and Mg-banding in recrystallized foraminifera. Geology 50 (7), 760–764.

Tachikawa, K., Sepulcre, S., Toyofuku, T., Bard, E., 2008. Assessing influence of diagenetic carbonate dissolution on planktonic foraminiferal Mg/Ca in the southeastern Arabian Sea over the past 450 ka: Comparison between Globigerinoides ruber and Globigerinoides sacculifer. Geochem. Geophys. Geosyst. 9 (4).

Tripati, A.K., Eagle, R.A., Thiagarajan, N., Gagnon, A.C., Bauch, H., Halloran, P.R., Eiler, J.M., 2010. 13C-18O isotope signatures and "clumped isotope" thermometry in foraminifera and coccoliths. Geochim. Cosmochim. Acta 74, 5697–5717.

Van Der Ploeg, R., Cramwinckel, M.J., Kocken, I.J., Leutert, T.J., Bohaty, S.M., Fokkema, C.D., Sluijs, A., 2023. North Atlantic surface ocean warming and salinization in response to middle Eocene greenhouse warming. Sci. Adv. 9 (4).

Zweng, M.M., Reagan, J.R., Seidov, D., Boyer, T.P., Locarnini, M.M., Garcia, H.E., Mishonov, A.V., Baranova, O.K., Weathers, K.W., Paver, C.R., Smolyar, I., 2019. World Ocean Atlas 2018, Volume 2: Salinity. Ref. NOAA Atlas NESDIS 82, pp. 50.